3D Iterative Reconstruction of High Resolution PET/CT Images using Anatomical Priors and Attenuation Correction

Juan E. Ortuño, George Kontaxakis, José L. Rubio, Pedro Guerra and Andrés Santos

***Abstract*—High resolution PET/CT tomographs provide anatomical CT images of small rodents co–registered with functional data. We present an algorithm for the reconstruction of PET images using the CT anatomical data to regularize the fully–3D OS–EM algorithm and correct for the attenuation effect. The penalty term is weighted by the cross–entropy between the prior image and an anatomical edge–preserving smoothed version of the previous iteration result. The penalty term reduces the noise amplification, which is a drawback of iterative OS–EM reconstruction algorithm, and improves edge resolution where anatomical variations exist, showing robustness against misalignments or other errors in the CT data. The attenuation correction factors are calculated by mapping the CT photon energy image to PET photon energy, followed by a forward projection with the same system matrix coefficients used in the reconstruction process. A 3D efficient implementation has been developed for a high resolution PET scanner composed of rotating planar detectors. The associated system matrix is precalculated with Monte Carlo methods that simulate physical effects not included in analytical models. The scanner geometry allows the use of axial and transaxial symmetries, and only the non–zero system matrix elements belonging to one quadrant of a central transaxial slice need to be precalculated and stored in sparse matrix format.**

***Index Terms*—PET, PET/CT, statistical reconstruction, anatomical information.**

I. Introduction

Statistical image reconstruction algorithms for positron emission tomography (PET) show superior image quality to analytic techniques, mainly due to the fact that they include an accurate system response model which can incorporate several physical parameters not included in analytical methods. Their high computational cost is the main drawback that has been partially solved with the development of fast converging algorithms, like the ordered-subsets expectation-maximization (OS–EM) algorithm [1], an accelerated version of the maximum-likelihood expectation-maximization ML–EM reconstruction method [2]. OS–EM algorithm is becoming the standard for the reconstruction in 3D high resolution emission computed tomography.

In addition to the intrinsic spatial resolution, the image quality is limited by the low number of collected coincidences, along with the fact that the system response can not be modeled in full detail. This leads to an increase of the noise level as iterations proceed, unless the iterative procedure is stopped early in order to guarantee an acceptable resolution/noise trade–off. Many regularization techniques have been proposed to overcome the noise propagation in iterative algorithms, such as Bayesian maximum a posteriori (MAP) formulations [3].

Multimodality PET/CT imaging offers the additional advantage of co–registered anatomical data that can be included as priors in PET reconstruction algorithm. The CT image, that represents mass attenuation values for a continuous x–rays range of energies, could improve the emission PET image by:

1) Correcting for attenuation without the need of a transmission acquisition.
2) Incorporating anatomical information in the penalty term for a spatially variant regularization of the statistical algorithm.

We have developed a 3D iterative reconstruction algorithm with spatially variant regularization based on CT co–registered anatomical data and CT-based attenuation correction. The proposed scheme has been adapted to a high resolution PET scanner designed for small animal studies. The system matrix was modeled with Monte Carlo methods including inter-crystal attenuation effects, and stored in an efficient sparse matrix format. The proposed method is a 3D ordered–subsets version of the minimum cross-entropy algorithm (MXE) [4] where the prior image model is weighted by a non-linear edge preserving operator over the anatomical image. In addition, the system matrix values are modified according to the attenuation coefficients obtained through the mapped CT scan.

II. Materials and Methods

A. Scanner geometry

The proposed reconstruction method has been designed for a small animal PET scanner composed of two pairs of planar detectors in coincidence mode. The distance between opposite detectors is 160 mm, while each detector is composed of a 28×28 array of LSO pixelated crystals of size $1.5\,\text{mm} \times 1.5\,\text{mm} \times 12\,\text{mm}$, assembled on a 100 μm thick matrix of plastic reflector. The detectors are mounted on a rotating gantry with 180° rotation span. The useful field of view (FOV) is of $44.8\,\text{mm} \times 44.8\,\text{mm} \times 44.8\,\text{mm}$.

Coincidences are binned in direct and oblique sinograms which organize the projection space as a function of four tuple (s, φ, θ, r), where s is the distance between the axial axis and the projection of the line of response (LOR) onto a transaxial plane; φ is the azimuthal angle; θ is the polar angle, and r is

This work has been partially supported by projects PI041494, TEC2004-07052-C02-02, CDTEAM and EMIL. Departamento de Ingeniería Electrónica (DIE), Universidad Politécnica de Madrid, Ciudad Universitaria s/n, 28040, Madrid, Spain. Corresponding author: Juan E. Ortuño, E-mail: juanen@die.upm.es.

the mean between the axial coordinates of the two crystals in coincidence.

The intrinsic resolution of the scanner is matched by employing a sampling scheme of 0.8 mm in s and r, 1.5° in φ, and with a total projection size of 55×120×28×28 sinogram bins.

B. Reconstruction algorithm

The MXE algorithm modifies the ML–EM algorithm adding a cross-entropy between the current image estimate and the prior image model, according to equation (1):

$$x_i^{(n+1)} = \frac{x_i^{(n)}}{\sum_j a_{ji}} \left[\sum_j \frac{y_j a_{ji}}{\sum_k a_{jk} x_k^{(n)}} - \beta \ln \left(\frac{x_i^{(n)}}{z_i^{(n-1)}} \right) \right] \quad (1)$$

where $x_i^{(n+1)}$ is the estimate of the activity concentration in pixel i at iteration $n+1$; a_{ji} represents the probability that a event generated within the volume covered by voxel i is registered by detector pair j; y_j denotes the number of events recorded in each detector pair; z_i is the prior model image at voxel i. The constant β controls the relative weight of the cross-entropy term.

The prior model includes the anatomical information obtained with a co–registered CT scan through an edge-preserving and spatially variant smoothing filter. This regularization term incorporates therefore the anatomical boundaries in the PET reconstruction process.

If β in (1) is set to zero, then the 3D OS–MXE algorithm becomes equivalent to the 3D OS–EM un–regularized expression, but when $\beta \to \infty$ the positivity constraints of the OS–EM algorithm are not satisfied. Thus a limit for β must be imposed to guaranteed the stability of the algorithm.

C. Smoothing filter

If a smoothed version of the image estimation in the previous iteration is chosen as the prior image model z in (1), the 3D OS–MXE algorithm will equally smooth the whole image, thus resulting in a loss of resolution with non–edge preserving regularization. The prior model should instead be capable of smoothing noisy regions and preserving aligned edges among PET and CT co–registered images.

A 3D improved version of the gradient inverse weighted smoothing filter (GIW) [5] has been applied: If m_i denotes the anatomical image value at voxel i, and the voxel r is included in the vicinity of i, denoted as $V(i)$, the absolute value of the gradient is defined as:

$$\delta_{i,r} = \begin{cases} 2 & \text{if } \|m_i - m_r\| = 0 \\ 1/\|m_i - m_r\| & \text{otherwise} \end{cases} \quad (2)$$

and the GIW filter over the functional image x has the following expression:

$$z_i = \kappa_i x_i + (1 - \kappa_i) \sum_{r \in V(i)} \omega_r x_r \quad (3)$$

where ω and κ parameters are given as follows:

$$\omega_r = \frac{\delta_{i,r}}{\sum_{r \in V(i)} \delta_{i,r}}, \quad \kappa_i = \sum_{r \in V(i)} \omega_r^2 \cdot \left(1 + \sum_{r \in V(i)} \omega_r^2 \right)^{-1} \quad (4)$$

The vicinity of i has been fixed to 26–neighborhood, i e., a $3 \times 3 \times 3$ kernel, for the experiments presented in this work.

D. Attenuation correction

If the material properties are known thanks to the anatomical CT image, a LOR can be corrected for attenuation with a multiplicative factor that modifies the probability value stored in the precalculated system model. In small animal tomographs for pre–clinical studies, the magnitude of the correction is much smaller than in clinical studies because the mean distance along attenuation material is much shorter that in humans, although it is still important to correct the data for quantitative analysis.

Since the linear attenuation coefficients (LAC) are energy dependent, those measured at low CT energies (acquired with a continuous x–ray energy spectrum from 10 KeV to 70 KeV) are firstly transformed onto the corresponding values of gamma rays PET energies, i e., 511 KeV. We use a logarithmic function to fit the data (see Table I, [6]).

TABLE I
TISSUE LINEAR ATTENUATION COEFFICIENTS

LAC (cm^{-1})	Adipose	Water	Soft tissue	Cortical bone
511 KeV	0.090	0.095	0.099	0.170
40 KeV	0.228	0.268	0.285	1.278

The attenuation correction factors are then obtained by a projection of the LORs though the attenuation map [7] resampled to match the low resolution of a PET image using cubic interpolation. The forward projection routine is the same that in the 3D reconstruction method, matching spatial resolution.

E. System matrix modeling

The set of a_{ji} values in (1), denoted as system matrix, is accurately modeled with Monte Carlo methods which include attenuation and scatter effects in the detector. The details are described in our previous work [8].

Practical implementation of the algorithm imposes the use of approximations where the majority of a_{ji} have zero values, and an efficient sparse–matrix storage that is read in sequential order during projection and back–projection iteration steps. However in the 3D case, the number of non–zero a_{ji} is too large to be efficiently handeled by a typical PC, and possible redundancies must be considered, i e., axial and transaxial system matrix symmetries [9].

The system matrix has an image size of $112 \times 112 \times 56$ voxels of [0.4, 0.4, 0.8] mm. The total number of a_{ji} elements in the matrix is $7.10 \cdot 10^{12}$, however its symmetries and high sparsity allows its representation in 557 MB of disk storage.

The voxel size is chosen at one quarter the size of the pixelated crystal dimension in the transaxial plane, to ensure that the intrinsic scanner resolution is matched, and half the size in the axial direction, which facilitates the application of parallel shift redundancies and axial reflection symmetries within one transaxial plane only [9]. The a_{ji} values obtained by Monte Carlo simulation are filtered to reduce variance and ordered in 10 subsets according to the φ value.

F. Data acquisition

The reconstruction scheme has been evaluated with the SimSET emission tomography simulation package [10], which includes scatter, attenuation, no–collinearity and positron range effects.

Coincidences from simulated studies were collected in list mode format, replacing the 3D sinogram binning module provided by SimSET by a custom version that doesn't evaluate depth of interaction resolution, but calculates the sinogram bin from the centers of the pixelated crystal with the highest probability to detect the photons.

The phantom shown in Fig. 1 was simulated to evaluate the noise characteristics, contrast recovery and resolution of the proposed algorithm. The background cylinder has a diameter of 36 mm and 45 mm in length, centered on the scanner axial axis. The lower part of the phantom contains a hot cylinder with twice the background activity concentration, as well as a cold cylinder without activity. Both cylinders have dimensions of 12 mm in diameter and 15 mm in length. The upper part of the phantom consists of five cylinders with 15 mm in length and diameters of 7.5, 6, 4.5, 3 and 1.5 mm. Their activity concentration was also chosen twice the background activity.

The attenuation was chosen equal to water or bone at 511 KeV, according to the Fig. 1. It can be noted that there are also anatomical boundaries without activity gradient for the purpose of evaluating the robustness of the reconstruction algorithm against CT information not correlated with functional PET regions.

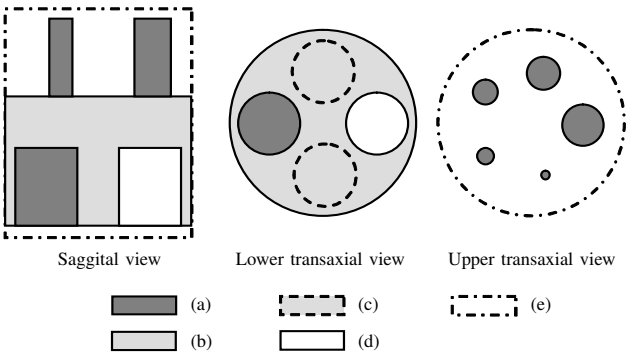

Fig. 1. Transverse and saggital views of the simulated phantom. Cylinders have the following relative activity densities and materials: (a) bone and activity $= 2\alpha$; (b) water and activity $= \alpha$; (c) bone and activity $= \alpha$; (d) bone and activity = 0; (e) water and activity = 0.

The second study simulated with SimSET consists of the cranial subset of the realistic Digimouse phantom [11] which includes a co–registered CT image, both sampled at 0.1 mm/voxel. To adjust to the FOV of the PET scanner the acquisition was restricted to include only the mouse head.

Radionuclide activity concentrations were chosen from each tissue mean value in the Digimouse PET image, except for the non–segmented zones, where the measured activity was reduced to get more contrast in our experiments. The attenuation volume required in SimSET simulations was obtained from the Digimouse atlas mapped at 44.7 KeV tissue attenuation coefficients.

The CT Digimouse scan consists of a 8 bit scaled image, that is mapped to the attenuation values at 40 KeV with the segmented atlas using the segmented co–registered image. In non–segmented images it should be necessary to estimate the tissue mean gray level values by an appropiate segmentation method.

III. RESULTS

In Fig. 2 the OS–EM and OS–MXE reconstructions of the phantom study are compared at different views. A higher degree of smoothing can be observed in the second one, while the edges aligned with anatomical interfaces are enhanced. There are no significant artifacts related to non–correlated CT and PET data. Quantitative results of the reconstructed

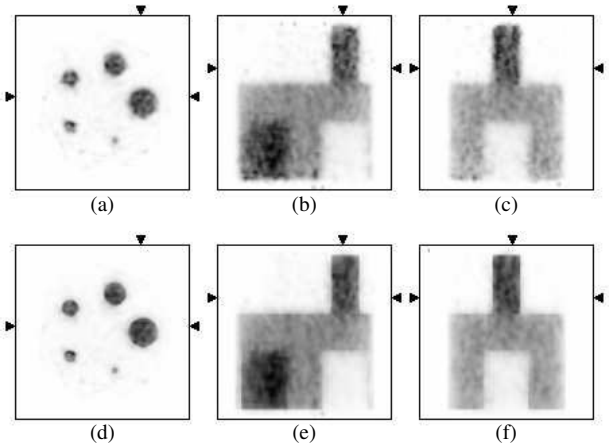

Fig. 2. Reconstructions of the phantom simulated with SimSET. (a),(b) and (c): transaxial, coronal and saggital sections of a 3D OS–EM reconstruction with MAP regularization, without anatomical information. (d),(e) and (f): 3D OS–MXE reconstruction. The same system matrix has been used in both images, using 10 subsets and 6 iterations

image quality are plotted in Table II. The measured parameters represent the percent contrast recovery for the hot cylinder (Q_H) and cold cylinder (Q_C), and the percent background variability [12]. The contrast recovery is slightly better in MXE reconstructions while noise level is reduced. Edge enhancement and contrast recovery can also be observed in Figs. 3 and 4, showing profiles along the OS–EM and OS–MXE images with $\beta = 0.01$ Finally, different views of the reconstructed mouse phantom are shown in Fig. 5. OS–MXE reconstruction is less noisy and is capable of delineating better those structures related to attenuation steps in CT image.

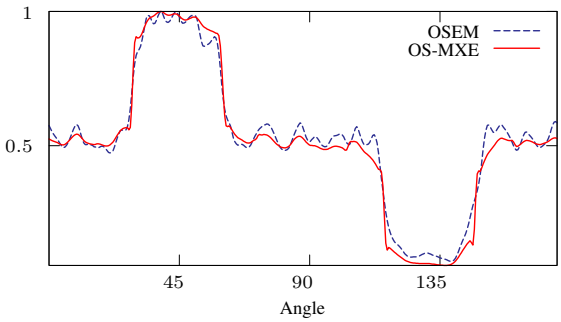

Fig. 3. Profile along a circular path 18 mm off the axial axis, crossing hot and cold cylinders of the inferior part of the phantom.

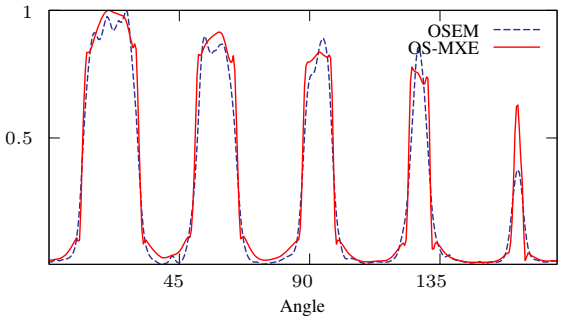

Fig. 4. Profile along a circular path 18 mm off the axial axis, crossing small cylinders located at the superior part of the phantom.

IV. Conclusions

A fully–3D OS–MXE reconstruction algorithm has been developed, implemented and evaluated for a high resolution rotating head PET scanner composed of two pairs of opposed planar pixelated blocks. The proposed scheme employs pre-calculated system matrix based on Monte Carlo methods and efficiently stored in disk with sparse–matrix format. The experiments performed with simulated phantoms show that the proposed algorithm improves the edge resolution as compared to 3D OS–EM reconstructions when there is a spatial correlation between anatomical and functional data, reducing at the same time the noise level within anatomical boundaries. As a result, a superior contrast recovery has been reported for these simulated phantoms. Within an adequate range of β values, there are no artifacts for the case of anatomical boundaries not related to activity variations in the functional data.

TABLE II
Contrast and Background Variability

β	Q_H	Q_C	Background Variability
– [a]	0.871	0.833	0.366
0.001[b]	0.877	0.847	0.312
0.005[b]	0.883	0.857	0.237
0.01 [b]	0.856	0.860	0.223

[a] 3D OS–EM algorithm, $\beta = 0$
[b] 3D OS–MXE algorithm

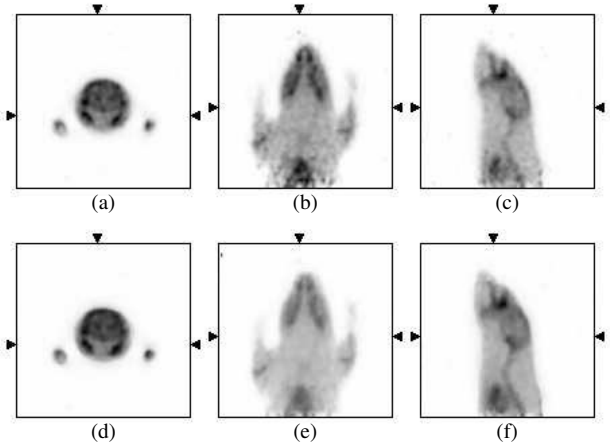

Fig. 5. Reconstructions after 6 iterations of the realistic mouse phantom simulated with SimSET. (a),(b) and (c): 3D OS–EM reconstruction with MAP regularization (transaxial, coronal and saggital sections). (d),(e) and (f): 3D OS–MXE reconstruction with CT anatomical priors.

References

[1] H. M. Hudson and R. S. Larkin, "Accelerated image reconstruction using ordered subsets of projection data," *IEEE Transactions on Medical Imaging*, vol. 13, no. 4, pp. 601–609, 1994.
[2] L. A. Shepp and Y. Vardi, "Maximum likelihood reconstruction in positron emission tomography," *IEEE Transactions on Medical Imaging*, vol. 1, no. 2, pp. 113–122, 1982.
[3] E. U. Mumcuoglu, R. M. Leahy, and S. R. Cherry, "Bayesian reconstruction of PET images: Methodology and performance analysis," *Physics in Medicine and Biology*, vol. 41, no. 9, pp. 1777–1807, 1996.
[4] B. A. Ardekani, M. Braun, B. F. Hutton, I. Kanno, and H. Iida, "Minimum cross-entropy reconstruction of PET images using prior anatomical information," *Physics in Medicine and Biology*, vol. 41, no. 11, pp. 2497–2517, 1996.
[5] X. Wang, "On the gradient inverse weighted filter," *IEEE Transactions on Signal Processing*, vol. 40, no. 2, pp. 482–484, 1992.
[6] P. L. Chow, F. R. Rannou, and A. F. Chatziioannou, "Attenuation correction for small animal PET tomographs," *Physics in Medicine and Biology*, vol. 50, no. 8, pp. 1837–1850, 2005.
[7] P. E. Kinahan, D. W. Townsend, T. Beyer, and D. Sashin, "Attenuation correction for a combined 3D PET/CT scanner," *Medical Physics*, vol. 25, no. 10, pp. 2046–2053, 1998.
[8] J. E. Ortuño, P. Guerra, J. L. Rubio, G. Kontaxakis, and A. Santos, "3D OSEM-based iterative image reconstruction for high resolution PET using precalculated system matrix," *Nuclear Instruments and Methods in Physics Research Section A*, vol. 569, no. 2, pp. 440–444, 2006.
[9] J. E. Ortuño, J. L. Rubio, P. Guerra, G. Kontaxakis, and A. Santos, "Multi-grid 3D-OSEM reconstruction technique for high resolution rotating-head PET scanners," in *Nuclear Science Symposium Conference Record*, vol 4. pp. 2215-2218, 2006.
[10] M. Ljungberg and S. E. Strand, "A Monte-Carlo program for the simulation of scintillation samera characteristics," *Computer Methods and Programs in Biomedicine*, vol. 29, no. 4, pp. 257–272, 1989.
[11] B. Dogdas, D. Stout, A. F. Chatziioannou, and R. M. Leahy, "Digimouse: a 3D whole body mouse atlas from CT and cryosection data," *Physics in Medicine and Biology*, vol. 52, no. 3, pp. 577–587, 2007.
[12] "NEMA standards publication NU 2-2001: Performace measurements of positron emission tomographs," Rosslyn, VA: National Electric Manufacturers Association, 2001.